7. I. Ya. Slonim, "Determination of particle sizes from light scattering: nomograms for determining the sizes of rod particles," Opt. Spektrosk., 9, No. 2, 244-247 (1960).
8. V. I. Klenin, S. Yu. Shchegolev, and V. I. Lavrushin, Characteristic Light-Scattering Functions for Dispersed Systems [in Russian], Saratov State Univ. (1977).
9. P. Ekwall and P. Holmberg, "The viscosities of sodium caprylate solution at 20°C measured with capillary viscometers," Acta Chem. Scand., 19, No. 2, 455-468 (1965).
10. I. L. Povkh et al., "The solubilizing capacity of aqueous solutions of cetylpyridinium chloride," Ukr. Khim. Zh., 43, No. 3, 275-279 (1978).
11. R. V. Kucher et al., "Effects of electrolytes on the second crystal concentration for micelle formation of sodium and calcium tetradecylsulfates," Ukr. Khim. Zh., 44, No. 8, 725-730 (1979).
12. Ya. Yu. Akhadov, Dielectric Properties of Pure Liquids [in Russian], Standartov, Moscow (1972).

FLOW DISTRIBUTION IN PERFORATED CHANNELS WITH A PERMEABLE END FACE

A. S. Nazarov, V. V. Dil'man, and S. P. Sergeev

UDC 532.545

The distribution of average velocity vs distance along a channel is given by a one-dimensional model based on the energy equation. An estimate is given of the suitability of the model in the presence of a developed turbulent velocity profile at the channel entrance.

An energy principle has previously been used to describe the average flow velocity distribution along the length of a channel with perforated walls [1, 2]. In a one-dimensional model, the differential equation describing the average parallel velocity distribution along the length of a perforated channel takes the form [2]

$$W''W' + aW'W + bW^2 = 0, \tag{1}$$

where

$$a = 2\frac{3-\varepsilon^2}{1+\xi}\left(\frac{\varphi L}{R}\right)^2;\ b = \frac{\lambda\varphi^2}{1+\xi}\left(\frac{L}{R}\right)^3.$$

The solution under the boundary conditions

$$X = 0,\ W = 1;\ X = 1,\ W = 0 \tag{2}$$

is given in [1] and corresponds to the case of a sealed end channel.

If the end face is not sealed but has many perforations and is permeable to liquid or gas, the boundary conditions will be as follows:

$$X = 0,\ W = 1;\ X = 1,\ W = W_\tau. \tag{3}$$

The solution of (1) with the boundary conditions (3) may be presented in parametric form as a system of three equations [3]

$$\ln W = \eta X + \frac{1}{2}\ln\frac{\theta_0^2+\theta_0\eta+\eta^2+a}{\theta^2+\theta\eta+\eta^2+a} + \frac{\eta}{2m}\left(\operatorname{arctg}\frac{2\theta+\eta}{2m} - \operatorname{arctg}\frac{2\theta_0+\eta}{2m}\right),$$

$$X = -\frac{\eta}{2(3\eta^2+a)}\left[\ln\left(\frac{\theta-\eta}{\theta_0-\eta}\right)^2\frac{\theta_0^2+\theta_0\eta+\eta^2+a}{\theta^2+\theta\eta+\eta^2+a}\right] + \frac{3\eta^2+2a}{2m(3\eta^2+a)}\left(\operatorname{arctg}\frac{2\theta_0+\eta}{2m} - \operatorname{arctg}\frac{2\theta+\eta}{2m}\right), \tag{4}$$

$$1 = -\frac{\eta}{2(3\eta^2+a)}\left[\ln\left(\frac{\theta_\tau-\eta}{\theta_0-\eta}\right)^2\frac{\theta_0^2+\theta_0\eta+\eta^2+a}{\theta_\tau^2+\theta_\tau\eta+\eta^2+a}\right] + \frac{3\eta^2+2a}{2m(3\eta^2+a)}\left(\operatorname{arctg}\frac{2\theta_0+\eta}{2m} - \operatorname{arctg}\frac{2\theta_\tau+\eta}{2m}\right),$$

Translated from Inzhenerno-Fizicheskii Zhurnal, Vol. 41, No. 6, pp. 1009-1015, December, 1981. Original article submitted September 30, 1980.

 0022-0841/81/4106-1304$07.50

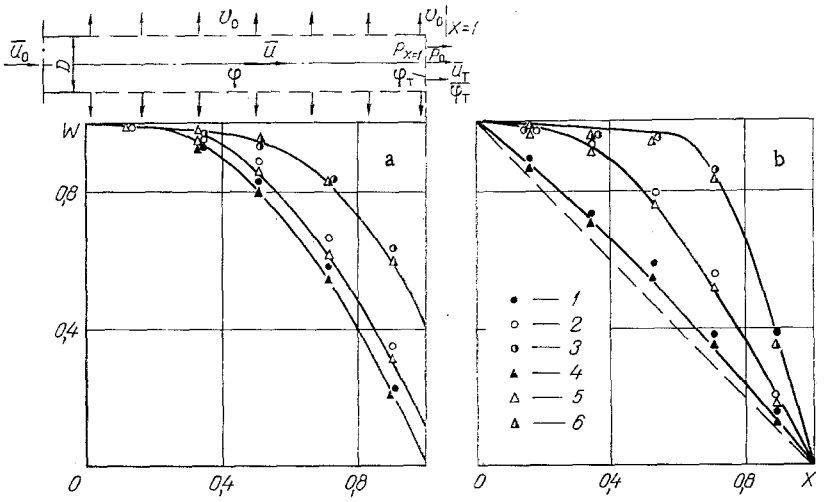

Fig. 1. Distribution of average parallel velocity along the length of a perforated channel with a permeable end face ($\varphi = 0.08$), curve a, and with a sealed end face, curve b. Curves 1-3 have a developed turbulent velocity profile at the entrance, whereas curves 4-6 are for a laminar flow. a: 1, 4) $\varphi_T = 0.05$; 2, 5) 0.2; 3, 6) 0.5; b: 1, 4) $\varphi = 0.04$; 2, 5) 0.08; 3, 6) 0.15.

where η is the real root of the cubic $\theta^3 + a\theta + b = 0$, and $m = (3/4\eta^2 + a)^{1/2}$.

The parameter $\theta = W'/W$ varies along the channel from θ_0 at the entrance to the perforated channel to θ_T at the permeable end face.

It is necessary to determine θ_T in order to solve the system of equations (4).

Consider Fig. 1a and the channel cross section immediately at the permeable end face ($X = 1$). At this section the static pressure may be considered independent of radius and equals $P|_{X=1}$. Analysis shows that the error introduced into the determination of P is less than 1%. The gas velocity in the perforations of the end face equals $\bar{u}_T/\varphi_T$. The equation for the gas efflux through the face into the external medium we will write in the form

$$\frac{P|_{X=1} - P_a}{\rho} = \frac{\xi_T}{\varphi_T^2}\frac{\bar{u}_T^2}{2}. \tag{5}$$

For the same cross section, the condition of gas efflux through the side walls of the perforated channels is determined by the following relation:

$$\frac{P|_{X=1} - P_a}{\rho} = \xi\frac{v_0^2|_{X=1}}{2}. \tag{6}$$

It follows from (5) and (6) that

$$\frac{\xi_T}{\varphi_T^2}\bar{u}_T^2 = \xi v_0^2|_{X=1}. \tag{7}$$

According to [4], the drag coefficient referred to the gas velocity in the holes may be expressed through the amount of open area

$$\xi = \left(1 - \varphi + \frac{\sqrt{2}}{2}\sqrt{1-\varphi}\right)^2. \tag{8}$$

Then Eq. (7) using (8) takes the form

$$\frac{v_0|_{X=1}}{\bar{u}_T} = \frac{1}{\varphi_T}\frac{1 - \varphi_T + \frac{\sqrt{2}}{2}\sqrt{1-\varphi_T}}{1 - \varphi + \frac{\sqrt{2}}{2}\sqrt{1-\varphi}}. \tag{9}$$

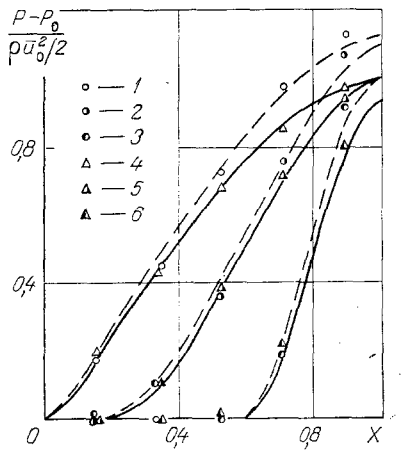

Fig. 2

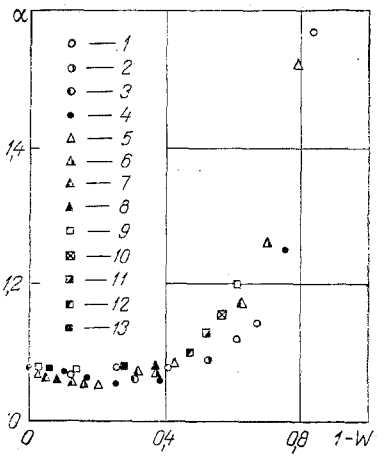

Fig. 3

Fig. 2. Pressure distribution along the length of a perforated channel with a dead end. In curves 1-3 there is a developed turbulent velocity profile but in curves 4-6 the flow is laminar. The parameter φ has the values 0.04 in curves 1, 4; 0.08 in 2, 5; and 0.15 in 3, 6.

Fig. 3. The change in the velocity correction in a perforated channel: 1-4) $\varphi = 0.04$; 5-8) 0.08; 9-13) 0.15; 1, 5, 9) $\varphi_T = 0$; 10) 0.05; 2, 6, 11) 0.1; 3, 7, 12) 0.2; 4, 8, 13) 0.5.

From the flux conservation equation $\operatorname{div} \vec{V} = 0$ at the cross section $X = 1$, we can write in dimensionless form

$$v_0|_{X=1} = -\frac{R}{2\varphi}\frac{\bar{u}_0}{L}(W')_T. \tag{10}$$

Substituting (10) into (9) and taking into consideration that $\bar{u}_T = W_T\bar{u}_0$, we obtain an equation for the desired quantity at the permeable end face of the channel

$$\theta_T = \frac{(W')_T}{W_T} = -\frac{2\varphi L\left(1-\varphi_T+\frac{\sqrt{2}}{2}\sqrt{1-\varphi_T}\right)}{\varphi_T R\left(1-\varphi+\frac{\sqrt{2}}{2}\sqrt{1-\varphi}\right)}. \tag{11}$$

The experimental data were taken with a cylindrical perforated channel with an inside diameter of 0.106 m and a length of 1.0 m. The open area of the side wall was made with 5-mm-diameter holes and had the values $\varphi = 0.04$, 0.08, and 0.15. The channel end face was covered either by a solid plate ($\varphi_T = 0$) or by one of a set of plates with 4-mm-diameter holes and open areas $\varphi_T = 0.05$, 0.1, 0.2, or 0.5.

In order to more accurately satisfy the assumption of the one-dimensional model, one must ensure a laminar longitudinal velocity profile at the entrance to the perforated channel. Such a profile was established with two grids attached to the entrance of the experimental region. The longitudinal velocity profiles at various cross sections along the length of the perforated channel were measured with pneumatic tubes which we moved radially in the range $0 < r/R < 0.99$. Experiments showed that the laminar velocity profile was maintained almost constant up to the end face of the channel.

It is interesting to estimate the degree to which a one-dimensional model may describe the distribution of a two-dimensional gas flow in a channel with porous walls. For this we applied a flow with a fully developed turbulent velocity profile to the entrance of the perforated channel. Hydrodynamic stabilization of the flow was ensured with a section of tube 40 diameters long. All experiments were conducted with a Reynolds number at the entrance to the experimental region of $Re_0 = 1.4 \times 10^5$. The average flow velocities at different cross sections along the length of the perforated channel were computed by integrating the measured velocity profiles.

In Fig. 1b experimental results are presented of the average longitudinal flow velocity distribution along a perforated channel for the case of a sealed end face and for various open areas of the side wall. The dashed line corresponds to a uniform distribution. The solid line was computed from Eq. (1) with boundary condition (2). With an increase of the open area of the side wall, the curves became more convex, which increases the degree of nonuniformity of the efflux velocity distribution along the channel length.

In Fig. 1a are shown the results of investigating the flow distribution along the length of the perforated channel ($\varphi = 0.08$) with different permeabilities for the end face. The dashed line is computed according to Eqs. (4) and (11).

As can be seen from Fig. 1, the model we have adopted on the basis of an energy principle well describes the one-dimensional flow in a perforated channel both with a sealed end face (which confirms the results of [5]) and also with a porous end face. Regarding the experimental points corresponding to the growth of the longitudinal velocity profile at the entrance, the fact that they are located primarily above the calculated curves, especially at the center of the channel, denotes a somewhat larger nonuniformity of the radial efflux velocity distribution in comparison with one-dimensional flow. Just the same pattern appears in Fig. 2, which illustrates the coincidence of the experimental and computed curves (dashed lines) of the static pressure in one-dimensional flow. With an increase in the velocity profile at the entrance, the measured values of static pressure increase toward the channel end face in comparison with the one-dimensional model. At the last measured channel cross section ($x = 0.88$) for $\varphi = 0.44$ the difference in the static pressure reaches 15%. A pressure increase in the downstream channel cross section leads to an increase of the radial velocity at the wall and, consequently, increases the nonuniformity of the efflux along the length of the channel.

To explain the discrepancy in the experimental results, one must take into account the additional kinetic energy which is introduced into the channel by a flow with a developed turbulent profile in comparison with laminar flow.

In [2] the energy equation for a stationary isothermal incompressible flow in a cylindrical channel with porous walls is written in the form

$$\pi R^2 \rho \frac{\partial}{\partial x}\left[\alpha_1 \frac{\bar{u}^3}{2} + \alpha_2 \bar{u}\left(\frac{v_0^2}{2} + \frac{P}{\rho}\right)\right] dx + 2\pi R \varphi \rho v_0 \left(\frac{\varepsilon^2 \bar{u}^2}{2} + \frac{v_0^2}{2} + \frac{P}{\rho}\right) dx = d\Phi. \tag{12}$$

The first and second terms on the left side of expression (12) are the longitudinal and radial energy fluxes through the side walls of the channel, respectively. The right side is the dissipation term, which may be represented in the form

$$d\Phi = -\lambda \rho \frac{\bar{u}^3}{8} 2\pi R dx. \tag{13}$$

In Eq. (12) α_1 and α_2 are average correction factors:

$$\alpha_1 = \int_0^{\pi R^2} u^3 d(\pi R^2)/\pi R^2 \bar{u}^3,$$

$$\alpha_2 = \int_0^{\pi R^2} \rho u \left(\frac{v^2}{2} + \frac{P}{\rho}\right) d(\pi R^2)/\rho \bar{u} \int_0^{\pi R^2} \left(\frac{v^2}{2} + \frac{P}{\rho}\right) d(\pi R^2).$$

In the expression for α_2, the quantity $(v^2/2 + P/\rho)$ is inside the integral. Considering that the static pressure P is practically constant across the channel cross section and that $P/\rho \gg v^2/2$, we may estimate that $v^2/2 + P/\rho = \text{const}$ and consequently that $\alpha_2 = 1$. The quantity α_1 for a developed turbulent profile does not equal 1. Furthermore, considering the comments regarding α_1 and α_2 and the fact of mass conservation $v_0 = -\frac{R}{2\varphi}\frac{d\bar{u}}{dx}$, by performing the differentiation in Eq. (12) and taking (13) into account, we obtain

$$\frac{3\alpha - \varepsilon^2}{2} \bar{u}' \bar{u}^2 + \frac{1}{2} \alpha' \bar{u}^3 + v_0 v_0' \bar{u} + \frac{P_{oc}'}{\rho} \bar{u} + \frac{\lambda'}{4R} \bar{u}^3 = 0. \tag{14}$$

In this and below the subscript 1 on α will be omitted.

If $\alpha = 1$, then Eq. (14) takes a form corresponding to the one-dimensional case (with a laminar velocity profile):

$$\frac{3-\varepsilon^2}{2}\bar{u}'\bar{u}^2 + v_0 v_0'\bar{u} + \frac{P_{la}'}{\rho}\bar{u} + \frac{\lambda}{4R}\bar{u}^3 = 0. \tag{15}$$

Computing from (14) Eq. (15) and performing a simple transformation, we obtain

$$2\left[\frac{P_{oc}-P_{la}}{\rho}\right]' = -\frac{1}{\bar{u}}[(\alpha-1)\bar{u}^3]'. \tag{16}$$

Transforming to dimensionless form, we may write

$$\frac{\partial}{\partial X}\left(\frac{P_{oc}-P_{la}}{\rho\bar{u}_0^2/2}\right) = -\frac{1}{W}\frac{\partial}{\partial X}[(\alpha-1)W^3]. \tag{17}$$

Integrating (17) we obtain a formula for the pressure distribution in a perforated channel for the case of a developed velocity profile at the entrance

$$\frac{(P-P_0)_{oc}}{\rho\bar{u}_0^2/2} = \frac{(P-P_0)_{la}}{\rho\bar{u}_0^2/2} - \int_0^X \frac{1}{W}\frac{\partial}{\partial X}[(\alpha-1)W^3]\,dX. \tag{18}$$

The first term on the right side of Eq. (18) represents the pressure distribution in one-dimensional flow and is shown in Fig. 2 (solid line). The second term allows for the two-dimensionality of the flow. This integral was computed on the basis of the experimental points at each measured cross section of the perforated channel for a developed velocity profile at the channel entrance. In Fig. 2 the dashed curves are computed from Eq. (18) and satisfactorily describe the experimental data corresponding to a developed velocity profile at the channel entrance.

The indicated analysis showed that the discovered discrepancy is mainly due to the neglect of two-dimensional flow in Eq. (1).

The error in the efflux velocity caused by the neglect of two-dimensional flow can be as large as 7.5%, while the error in the static pressure is up to 15%.

With this limitation, the one-dimensional model may evidently be applied to a description of the velocity distribution along the length of a perforated cylindrical channel for flows with an initial profile taking any possible form with locally stable flow from a laminar profile to the profile of fully developed turbulence. If a refinement is needed, one should make further use of Eq. (18) and the relation $\alpha = f(W)$ (Fig. 3).

The experimental results in perforated channels with a porous end face are well described by the presented model with modified boundary conditions. This circumstance allows the model to be used in solving many practically important problems encountered in development of chemical reactors, ventilator systems, filters, etc.

NOTATION

u, local longitudinal velocity, m/sec; $\bar{u}$, longitudinal mean velocity over the cross section, m/sec; $\bar{u}_0$, mean velocity in the starting cross section of the channel, m/sec; $\bar{u}_T$, mean velocity on the permeable end face of the channel, m/sec; W, dimensionless mean longitudinal velocity; W_T, dimensionless mean velocity on the permeable end face, $W_T = \bar{u}_T/\bar{u}_0$; v_0, radial velocity in the holes of the side channel surface, m/sec; P, static pressure in the channel, N/m^2; P_0, static pressure in the starting channel cross section, N/m^2; P_a, medium pressure outside the channel, N/m^2; P', pressure derivative along the longitudinal coordinate, $N/m^2 \cdot m$; v_0', radial velocity derivative along the longitudinal coordinate, m/sec; x, r, longitudinal and radial coordinates, m; L, R, channel length and radius, m; X, dimensionless longitudinal coordinate; $X = x/L$; W', W'', appropriate derivatives along the dimensionless coordinate; φ, part of a free section of the side channel surface; φ_T, part of a free section of the channel end face; ξ, resistance coefficient at efflux through the side channel walls; ξ_T, resistance coefficient at efflux through the channel end face; λ, friction coefficient for the flow moving in the solid wall channel; ρ, medium density, kg/m^3; $\varepsilon = V_X/\bar{u}$, ratio of the projection of the suction velocity through the side surface onto the longitudinal channel axis to the mean longitudinal velocity in this channel cross section. Indices: *la*, laminar profile; oc, developed turbulent inlet profile.

LITERATURE CITED

1. V. V. Dil'man, S. P. Sergeev, and V. S. Genkin, "The description of current flow in a channel with porous walls based upon the energy equation," Teor. Osn. Khim. Tekhnol., 5, No. 4, 564-571 (1971).
2. S. P. Sergeev, V. V. Dil'man, and V. S. Genkin, "The flow distribution in channels with porous walls," Inzh.-Fiz. Zh., 27, No. 4, 588-595 (1974).
3. E. Kamke, Handbook of Ordinary Differential Equations [in German], Chelsea Publ.
4. I. E. Idel'chik, Aerodynamics of Commercial Apparatus [in Russian], Énergiya, Moscow—Leningrad (1964).
5. V. S. Genkin, V. V. Dil'man, and S. P. Sergeev, "Distribution of a gaseous flow in a channel with porous walls," Gazovoe Delo, No. 7, 10-13 (1972).

DIAGNOSIS OF RHEOLOGICAL PROPERTIES OF VISCOELASTIC—PLASTIC MEDIA DURING THEIR FLOW IN PIPES

R. M. Sattarov

UDC 532.595.2+135

A method is proposed for diagnosing the viscoelastic—plastic properties of a medium.

Methods are available [1-3] for determining the relaxation properties of viscoelastic—plastic media, but the models used in these papers are generally not justified. Because of the complexity of the internal structure of such media, this justification is very difficult. Therefore, methods permitting first a reliable diagnosis of the internal structure of such media and then a determination of their parameters are of important theoretical and practical interest for the analysis and optimization of technological processes related to the flow of viscoelastic—plastic media in pipes and channels.

1. Let us consider pipe flow of a viscoelastic—plastic medium whose rheological equation is described by the following model:

$$\theta\frac{\partial\tau}{\partial t}+\tau-\tau_0=\mu\left(\frac{\partial V}{\partial r}+\lambda\frac{\partial^2 V}{\partial t\partial r}\right).$$

In writing this relation it is assumed that the velocity gradient and the stress are stabilized along the length.

It should be noted that this model was employed in [4] to describe bituminous mineral conglomerates such as asphalt concretes and their components.

The differential equations of motion for a viscoelastic—plastic medium in an elastic pipe have the form [1]

$$\left.\begin{aligned}\theta\frac{\partial^2 W}{\partial t^2}+(1+2a\lambda)\frac{\partial W}{\partial t}+2aW+\frac{2\tau_0}{R}=-\frac{1}{\rho}\left(\frac{\partial P}{\partial z}+\theta\frac{\partial^2 P}{\partial t\partial z}\right),\\ \rho c^2\frac{\partial W}{\partial z}=-\frac{\partial P}{\partial t},\\ 2a=8\mu/\rho R^2.\end{aligned}\right\}\qquad(1)$$

The diagnosis of the viscoelastic—plastic properties of a medium is based on the solution of the differential equations (1) or, under certain assumptions, on the solution of the first of these equations. By using calculated moments the dependence of certain relations of the moments type on parameters characterizing the viscoelastic properties of the medium can be written in analytic form, and a harmonic analysis can be made.

M. Azizbekov Azerbaidzhan Institute of Petroleum and Chemistry, Baku. Translated from Inzhenerno-Fizicheskii Zhurnal, Vol. 41, No. 6, pp. 1016-1026, December, 1981. Original article submitted December 23, 1980.